2008 IEEE International Conference on
Robotics and Automation
Pasadena, CA, USA, May 19-23, 2008

A Robotic Finger Equipped with an Optical Three-axis Tactile Sensor

M. Ohka, N. Morisawa, H. Suzuki, J. Takata, H. Koboyashi, and H. B. Yussof, *Member*, *IEEE*

Abstract— **In a previous paper we developed an optical three-axis tactile sensor that can acquire normal and shearing forces to be mounted on a robotic finger. Normal and shearing forces applied to the sensing element were detected separately; when we examined the repeatability of the present tactile sensor with 1,000 loading-unloading cycles, the respective error of the normal forces was 2%. In the present paper, the three-axis tactile sensor is mounted on a robotic finger of three degrees of freedom to evaluate it for dexterous hands. A series of three kinds of experiments were performed. First, the robotic hand touches and scans flat specimens to evaluate the sensing ability of the friction coefficient. Second, it detects the contour of parallelepiped and cylindrical objects. Finally, it manipulates a parallelepiped case put on a table by sliding it on the table. Since the present robotic hand was able to perform the above three tasks with appropriate precision, we expected that it would be applicable to dexterous hands in subsequent studies.**

I. Introduction

Since a three-axis tactile sensor can simultaneously detect normal and shearing forces, its sensing ability for detecting contact physics caused between an object and a finger surface is superior to other tactile sensors[1]-[5]. It can provide tactile information for material handling[6][7]. Regarding flexible and impact resistant surfaces as the most important, we improved conventional optical waveguide type tactile sensors[8]-[12] to develop an optical three-axis tactile sensor[13][14]. In a previous paper, we developed a hemispherical tactile sensor for general-purpose use with our three-axis tactile sensor that we intend to mount on the fingertips of a multi-fingered hand. When we examined the repeatability of the present tactile sensor with 1,000 load-unload cycles, the respective error of the normal and shearing forces was 2 and 5% to evaluate the basic characteristics needed for application to robotic dexterous hands.

On the other hand, so far several researchers have tried to mount tactile sensors on robotic multi-fingered hands to enhance manipulation and to stabilize grasping objects. Kaneko et al.[11] and Maekawa et al.[12] formulated dynamics including tactile information obtained by a conventional optical waveguide type tactile sensor mounted on the fingertip. These studies are important milestones because they showed the effectiveness of tactile information on multi-fingered hands.

The robotic hand can obtain differences in the object's attitude, friction coefficient, and subtle surface unevenness, if a three-axis tactile sensor is used instead of the conventional tactile sensor. Therefore the application area will be spread by the equipment of the three-axis tactile sensor. Especially in the case of humanoid robots, grasping slippery or flexible objects is required in living environments in contrast to industrial robots that handle standardized objects in controlled environments. Since the three-axis tactile sensor is effective in such cases, its importance will increase with improvement of humanoid robots.

In the present paper, we develop a robotic finger equipped with a three-axis tactile sensor as the first step of a series of studies in which we will develop a dexterous multi-fingered hand equipped with a three-axis tactile sensor. The present robotic hand possesses three motorized joints and a three-axis tactile sensor on each fingertip. We developed software to control the robotic finger based on resolved motion rate control. To exploit the present results for the multi-fingered hand in subsequent studies, we performed experiments on such basic motions as surface scanning and object manipulation. These experiments are conducted to obtain basic data for object recognition and stable grasping in multi-fingered robotics, because a robot should obtain shape and surface condition of the object before grasping it.

II. Three-axis Tactile Sensor

Figure 1 shows a schematic view of the present tactile processing system that explains the sensing principle. The present tactile sensor is composed of a CCD camera, an acrylic dome, a light source, and a computer. The light emitted from the light source is directed into the acrylic dome. Contact phenomena are observed as image data, which are acquired by the CCD camera and transmitted to the computer to calculate the three-axis force distribution. The sensing element presented in this paper is comprised of a columnar feeler and eight conical feelers, as shown in Fig. 2. The sensing elements, which are made of silicone rubber (Fig. 1), are designed to maintain contact with the conical feelers and the acrylic dome and to make the columnar feelers touch an object. Each columnar feeler features a flange that fits into a

M. Ohka is with the Graduate School of Information Science, Nagoya University, Furo-cho, Chikusaku, Nagoya 464-8601, Japan (phone: 81-52-789-4861; fax: 81-52-789-4800; e-mail: ohka@ is.nagoya-u.ac.jp).
N. Morisawa is with Graduate School of Engineering, Nagoya University.
H. Suzuki is with Honda Motor Co., Ltd., Japan
J. Takata is with the Olympus Corporation, Japan.
H. Kobayashi is with the Toyota Industry Cooperation, Japan.
H. B. Yussof is with the Graduate School of Information Science, Nagoya University, Japan (hanafiah@nuem.nagoya-u.ac.jp).

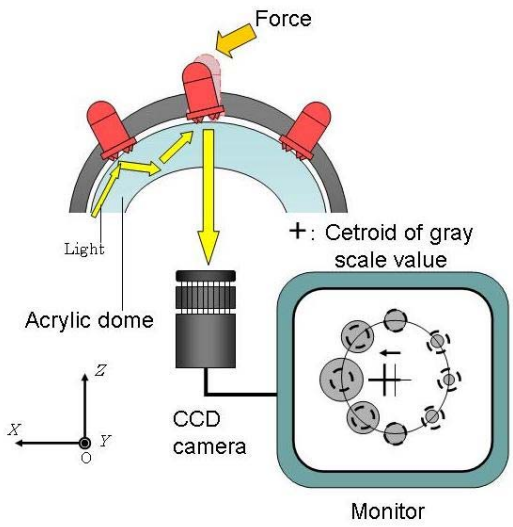

Fig. 1 Principle of three-axis tactile sensor

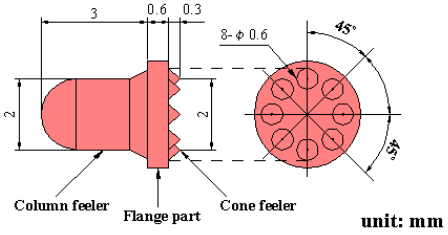

Fig. 2 Sensing element

counter bore portion in the fixing dome to protect the columnar feeler from horizontal displacement caused by shearing force.

When the three components of the force vector, F_x, F_y, and F_z, are applied to the tip of the columnar feeler, contact between the acrylic dome and the conical feelers is measured as a distribution of gray-scale values, which are transmitted to the computer. F_x, F_y, and F_z values are calculated using integrated gray-scale value G and the horizontal displacement of the centroid of gray-scale distribution $\boldsymbol{u} = u_x \boldsymbol{i} + u_y \boldsymbol{j}$ as follows:

$$F_x = f(u_x), \quad (1)$$

$$F_y = f(u_y), \quad (2)$$

$$F_z = g(G), \quad (3)$$

where $\boldsymbol{i}$ and $\boldsymbol{j}$ are orthogonal base vectors of the x- and y-axes of a Cartesian coordinate, respectively, and $f(x)$ and $g(x)$ are approximate curves estimated in calibration experiments.

We are currently designing a multi-fingered robotic hand for general-purpose use in robotics. The robotic hand includes links, fingertips equipped with the three-axis tactile sensor, and micro actuators (YR-KA01-A000, Yasukawa). Each micro actuator, which consists of an AC servo-motor, a harmonic drive, and an incremental encoder, is particularly developed for application to a multi-fingered hand.

Since the tactile sensors must be fitted to a multi-fingered hand, we are developing a fingertip that includes a

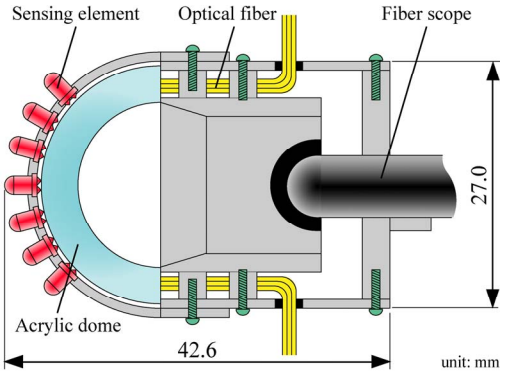

Fig. 3 Fingertip including three-axis tactile sensor

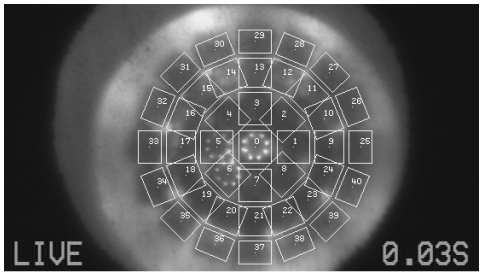

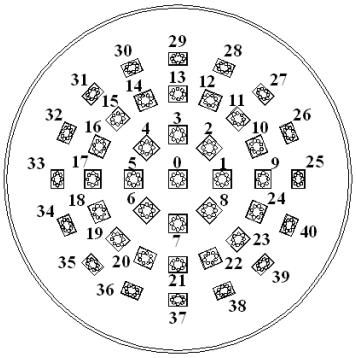

Fig. 4 Image data obtained by CCD camera and address of sensing elements

hemispherical three-axis tactile sensor. The fingertip and the three-axis tactile sensor are united, as shown in Fig. 3.

The sensing element of the tactile sensor is identical as the previously described element depicted in Fig. 2. Sensing elements are arranged on the acrylic dome in a concentric configuration. The acrylic dome is illuminated along its edge by optical fibers connected to a light source. Image data consisting of bright spots caused by the feelers' collapse are retrieved by an optical fiber scope connected to the CCD camera.

Image data acquired by the CCD camera are divided into 41 sub-regions (Fig. 4). The dividing procedure, digital filtering, integrated gray-scale values, and centroid displacement are processed on an image processing board.

Since the image warps due to projection from a hemispherical surface (Fig. 4), software installed on the computer modifies the warped image data and calculates G,

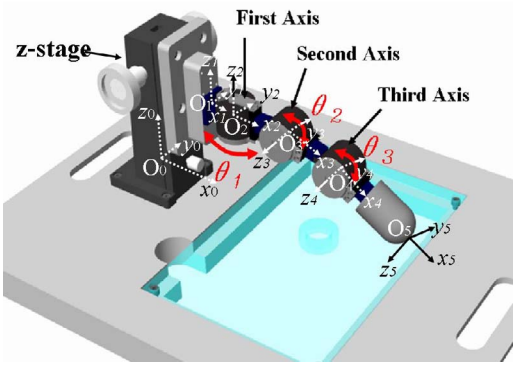

Fig. 5 Robotic finger equipped with a three-axis tactile sensor

u_x, and u_y to obtain the three-axis force applied to the tip of the sensing element using Eqs. (1)-(3).

III. Robotic Finger

As shown in Fig. 5, the present robotic finger has three movable joints. The frame of the workspace is set on the bottom of the z-stage. The kinematics of the present hand is derived according to Denabit-Hartenberg notation shown in Fig. 5. The frame of the workspace is defined as O-*xyz*. The frames of Oi-$x_i y_i z_i$ ($i = 0,2,\cdots,5$) (in the following, O-*xyz* is used instead of O_0-$x_0 y_0 z_0$) are attached on each joint, the basement of the z-stage, or the fingertip, as shown in Fig. 5. The velocities of the micro actuators ($\dot{\boldsymbol{\theta}} = \begin{pmatrix}\dot{\theta}_1 & \dot{\theta}_2 & \dot{\theta}_3\end{pmatrix}$) are calculated with

$$\dot{\boldsymbol{\theta}} = \mathbf{J}^{-1}(\boldsymbol{\theta})\dot{\mathbf{r}} \tag{4}$$

to satisfy specified velocity vector $\dot{\mathbf{r}}$ ($= \begin{pmatrix}\dot{x} & \dot{y} & \dot{z}\end{pmatrix}$), which is calculated from the planed trajectory. Jacobian $\mathbf{J}(\boldsymbol{\theta})$ is obtained by the kinematics of the robotic hand as follows:

$$\mathbf{J}(\boldsymbol{\theta}) = \begin{bmatrix} -R_{13}(l_2 + l_3 c_2 + l_4 c_{23}) & l_3(R_{11}s_3 + R_{12}c_3) + l_4 R_{12} & R_{12} l_4 \\ -R_{23}(l_2 + l_3 c_2 + l_4 c_{23}) & l_3(R_{21}s_3 + R_{22}c_3) + l_4 R_{22} & R_{22} l_4 \\ -R_{33}(l_2 + l_3 c_2 + l_4 c_{23}) & l_3(R_{31}s_3 + R_{32}c_3) + l_4 R_{32} & R_{32} l_4 \end{bmatrix}, \tag{5}$$

where

$$\begin{bmatrix} R_{11} & R_{12} & R_{13} \\ R_{21} & R_{22} & R_{23} \\ R_{31} & R_{32} & R_{33} \end{bmatrix} = \begin{bmatrix} a_{11}c_{23} + a_{13}s_{23} & -a_{11}s_{23} + a_{13}c_{23} & -a_{12} \\ a_{21}c_{23} + a_{23}s_{23} & -a_{21}s_{23} + a_{23}c_{23} & -a_{22} \\ a_{31}c_{23} + a_{33}s_{23} & -a_{31}s_{23} + a_{33}c_{33} & -a_{32} \end{bmatrix},$$

$$\begin{bmatrix} a_{11} & a_{12} & a_{13} \\ a_{21} & a_{22} & a_{23} \\ a_{31} & a_{32} & a_{33} \end{bmatrix} = \begin{bmatrix} c\phi_1 c_1 + s\phi_1 s\phi_2 s_1 & -c\phi_1 s_1 + s\phi_1 s\phi_2 s_1 & s\phi_1 c\phi_2 \\ c\phi_2 s\phi_1 & c\phi_2 s\phi_1 & -s\phi_2 \\ -s\phi_1 c_1 + s\phi_1 s\phi_2 s_1 & s\phi_1 s_1 + c\phi_1 s\phi_2 c\phi_1 & c\phi_1 c\phi_2 \end{bmatrix}$$

$c_i \equiv \cos\theta_i$, $s_i \equiv \sin\theta_i$, $c\phi_i \equiv \cos\phi_i$, $s\phi_i \equiv \sin\phi_i$,

$c_{ij} \equiv \cos(\theta_i + \theta_j)$, $s_{ij} \equiv \sin(\theta_i + \theta_j)$, ($i$; $j = 1, 2, 3$). (6)

In the above equations, the rotations of the first frame around the x_0- and y_0-axes are denoted as ϕ_1 and ϕ_2, respectively. The distance between the origins of the *m*-th and *m*+1-th frames is denoted as l_m. The joint angles of the micro actuators are θ_1, θ_2, and θ_3 (Fig. 5).

Position control of the fingertip is performed based on resolved motion rate control. In this control method, joint angles are assumed at the first step, and displacement vector $\mathbf{r}_0$ is calculated with kinematics. Adjustment of joint angles is obtained by Eq. (4) and the difference between $\mathbf{r}_0$ and objective vector $\mathbf{r}_d$ to modify joint angle $\boldsymbol{\theta}_1$ at the next step. The modified joint angle is designated as the current angle in the next step, and the above procedure is repeated until the displacement vector at *k*-th step $\mathbf{r}_k$ coincides with objective vector $\mathbf{r}_d$ within a specified error. That is, the following Eqs. (9) and (10) are calculated until $|\mathbf{r}_d - \mathbf{r}_k|$ becomes small enough:

$$\dot{\mathbf{r}}_k = \mathbf{J}\dot{\boldsymbol{\theta}}_k \tag{9}$$

$$\boldsymbol{\theta}_{k+1} = \boldsymbol{\theta}_k - \mathbf{J}^{-1}(\mathbf{r}_d - \mathbf{r}_k) \tag{10}$$

IV. Evaluation Experiments

A. Scanning on Flat Surface

In subsequent studies, we will attempt to develop a multi-fingered hand composed of the present robotic finger and perform object recognition and object manipulation tests using the hand. To exploit the present results for the multi-fingered hand in subsequent studies, we perform experiments on such basic motions as surface scanning and object manipulation.

First, in scanning on a flat surface, sensing element (#00) located on the vertex of the tactile sensor is made to perpendicularly contact with a flat table by adjusting angles θ_2 and θ_3. After that, a z-stage equipped with a robotic finger is adjusted to obtain appropriate contact force (0.1 N). Precision abrasive paper (produced by Sumitomo 3M) is mounted on the table. In this experiment, three kinds of abrasive paper, 1, 30, and 60 μ m, were adopted as specimens. To examine the dependence of friction coefficient on scanning speed, we chose three speeds: 1.4, 6.2, and 25 mm/sec.

B. Contour Tracing

In contour tracing, the robotic finger moves linearly and traces the object contour after it touches the object contour (Fig. 6). To realize this behavior with a simple algorithm, functions are shared among sensing elements. In this experiment, the robotic finger seeks the table with a linear downward motion before the contour tracing mode. If sensing element #00 accepts the normal force that exceeded 0.2 N, the robotic finger judges that it has reached the table and designates element #00 and the neighboring elements as a

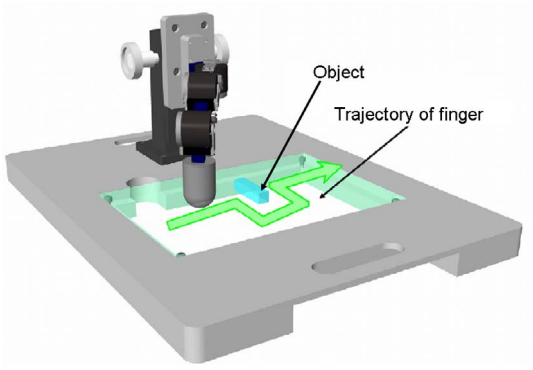

Fig. 6 Contour detection test

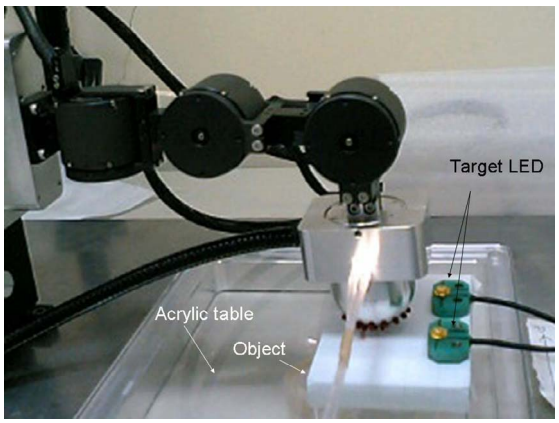

Fig. 7 Object manipulation

table detector. After finding the table, the robotic finger moves 5 mm upward and switches to the contour tracing mode. Since the fingertip orientation maintains a perpendicular direction to the table, sensing elements touch the contour of the object, except for element #00 and the neighboring elements.

During the contour tracing mode, if one of the sensing elements accepts the normal force that exceeded 0.3 N, the robotic finger comes off the object side surface and moves five mm from the surface. Then it moves linearly 5 mm in a vertical direction against the coming off direction. Then it approaches the object's surface again. The above cyclic manner is repeated to trace the object contour until the robotic finger returns to the designed trajectory.

C. Object Manipulation

If slippage occurs between a finger and an object, a robotic hand cannot manipulate the object without any control based on acquired slippage information. In object manipulation tests, we are attempting to check its capability to acquire slippage information using one-finger manipulation.

The robotic finger moves the parallelepiped object, which is put on the acrylic table (Fig. 7). Since the object is only put on the table, it is moved based on finger movement. During this manipulation, if the time derivative of the shearing force caused on the tactile sensor exceeds a specified threshold,

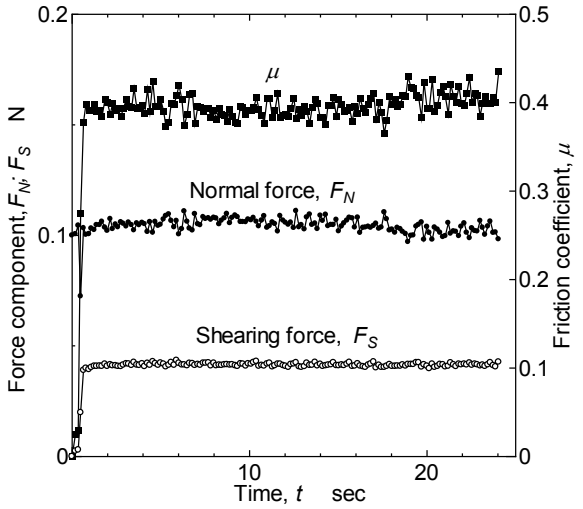

Fig. 8 Variation in force components and friction coefficient during scanning test (abrasive paper of 1 μ m and velocity of 6.2 mm/sec)

slippage is assumed, and the finger moves slightly downward to increase compressive force. Since the sensing element is made of silicone rubber, friction between the finger and the object can be increased without considerably increasing friction between the object and the table.

In this experiment, the robotic finger moves along a rectangular trajectory, and the object's movement is measured by a position sensitive detector (PS1100, Toyonaka Kenkyusyo, Co.).

V. Experimental Results and Discussion

A. Scanning on Flat Surface

First, we show variations in normal force, shearing force, and friction coefficient obtained during scanning in Fig. 8 to examine the dynamic characteristics of the tactile sensor. Figure 8 shows the case of 1 μ m and 6.2 mm/sec.

Shearing force starts at zero because it is not applied at zero speed. After the start, it increases abruptly to reach a constant value. Normal force almost shows a constant value. The coefficient of friction almost shows a constant value except near the origin. The mean value of the friction coefficient is 0.39. Friction coefficients for 30 and 60 μ m abrasive paper are 0.40 and 0.53, respectively.

Next, variation in friction coefficient against variation in scanning velocity is shown in Fig. 9. In this experiment, 1 μ m abrasive paper is adopted as a specimen and eight trials are performed for each scanning speed. As shown in Fig. 9, variation in friction coefficient decreases slightly with an increase of scanning velocity. Since cutting resistance decreases with an increase of cutting speed in grinding theory, we assume that this effect will arise in this experiment.

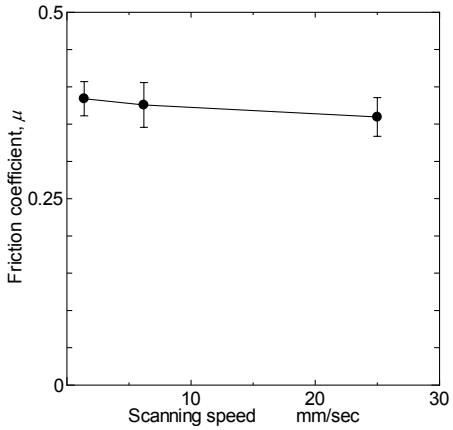

Fig. 9 Dependence of friction coefficient on scanning velocity

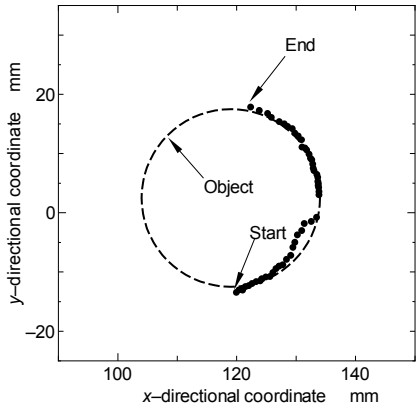

Fig. 10 Contour tracing for cylindrical surface

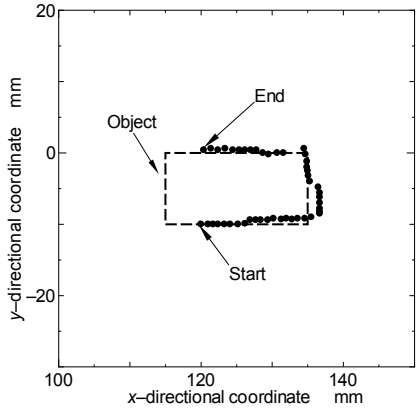

Fig. 11 Contour tracing for parallelepiped surface

B. Contour Tracing

Contour tracing tests for cylindrical and parallelepiped objects are shown in Figs. 10 and 11, respectively. Maximum deviation from the desired trajectory is about 3.6 mm for Fig. 10. The disconnected portion on the trajectory is caused by the searching process. Based on the present program, since the finger's motion is limited to the *x*- or *y*-direction for programming simplicity, tangential touching causes lost contour trajectory. At that time, the robotic finger searches the contour by a small square of trajectory 10 times 10 mm until it finds the contour again. Except for the above deviation and the disconnected portion, the robotic finger traces the cylinder's contour.

On the other hand, since the parallelepiped object's contour is composed of straight lines, exploring precision is higher than for the cylinder. However, since it has corners, it loses track of the contour at the corner. Except for corners, maximum deviation from the contour is 2.7 mm.

C. Object Manipulation

Figure 12 shows the trajectory and attitude of the manipulated object. To see the attitude easier, the parallelepiped object is shown as 1/10 size in Fig. 13. As shown in Fig. 12, the object moves along the desired trajectory with considerable deviation. To analyze slippage phenomenon, variations in normal force and shearing force derivatives are shown in Fig. 13. In this experiment, since sensor elements #00 and #07 emit rather large signal compared to elements #01, #03, #05, which touch the surface, their variations are shown in Fig. 13. To show the relationship between the representative points of Figs. 12 and 13, corresponding points are shown in both figures as identical characters.

In this experiment, since finger moving starts when the compressive force exceeds 0.5 N at point A, normal force abruptly decreases just after point A in terms of the inclination of the sensing element. Since the present robotic finger only possesses three degrees of freedom and cannot control its inclination, the contact point is changed. Consequently, just after point B's normal force of element #00 decreases, the normal force of element #07 increases.

Next, we examine the time derivative of the shearing force in Fig. 13. If the derivative vibration is examined on the segments, the derivative on BC, CD, DE, and EF is larger than on AB. This result means that slippage on BC, CD, DE, and EF is more considerable than on AB. Consequently, deviation after point C becomes considerable in terms of the slippage to cause the marked deviation on segment CD from the desired trajectory.

Through the above three experimental results, the present robotic finger possesses sensing ability for acquiring the friction coefficients of the object surface, the contour object, and the slippage phenomenon, which are useful bits of information for a multi-fingered hand.

VI. CONCLUSION

In the present paper, a three-axis tactile sensor was mounted on a robotic finger of three degrees of freedom to evaluate the tactile sensor for dexterous hands. In a series of experiments, three kinds of experiments were performed. First, the robotic hand touches and scans flat specimens to evaluate its friction coefficient. Second, it detects the contours of parallelepiped and cylindrical objects. Finally, it manipulates a parallelepiped case put on a table by sliding it.

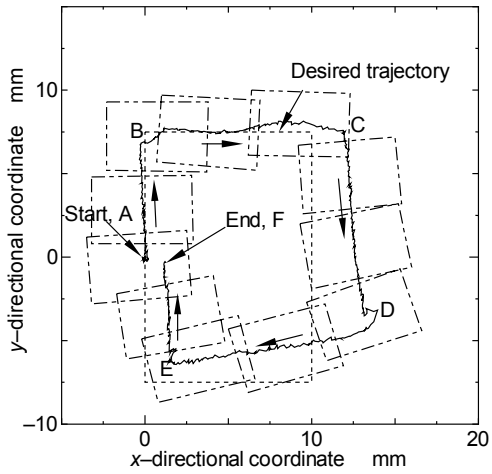

Fig. 12 Contour tracing for parallelepiped surface

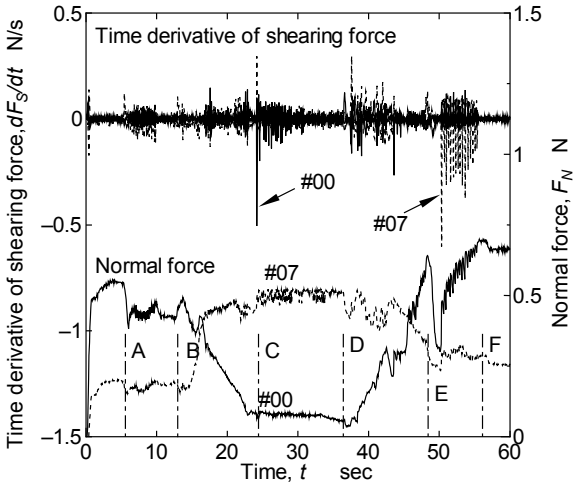

Fig. 13 Time derivative of shearing force in object manipulation

Since the present robotic hand was able to perform the above three tasks with appropriate precision, we expected that the hand is applicable to the dexterous hand in subsequent studies.

ACKNOWLEDGMENT

This study was partly supported by fiscal 2006 grants from the Ministry of Education, Culture, Sports, Science and Technology (No. 18656079).

REFERENCES

[1] Raibert, H. M. and Tanner, J. E., "Design and Implementation of a VSLI Tactile Sensing Computer," Int. J. Robotics Res., Vol. 1-3, 1982, 3-18.

[2] Hackwood, S., Beni, G., Hornak, L. A., Wolfe, R. and Nelson, T. J., "Torque-Sensitive Tactile Array for Robotics," Int. J. Robotics Research, Vol. 2-2, 1983, pp. 46-50.

[3] Dario, P., Rossi, D.D., Domenci, C. and Francesconi, R., "Ferroelectric Polymer Tactile Sensors with Anthropomorphic Features," Proc. 1984 IEEE Int. Conf. On Robotics and Automation, 1984, pp. 332-340.

[4] Novak, J. L., "Initial Design and Analysis of a Capacitive Sensor for Shear and Normal Force Measurement," Proc. of 1989 IEEE Int. Conf. on Robotic and Automation, 1989, pp. 137-145.

[5] Nicholls, H. R. & Lee, M. H., "A Survey of Robot Tactile Sensing Technology," Int. J. Robotics Res., Vol. 8-3, 1989, pp. 3-30.

[6] Ohka, M. et al., "Tactile Expert System Using a Parallel-fingered Hand Fitted with Three-axis Tactile Sensors," JSME Int. J., Series C, Vol. 37, No. 1, 1994, pp. 138-146.

[7] Takeuchi, S., Ohka, M., and Mitsuya, Y., "Tactile Recognition Using Fuzzy Production Rules and Fuzzy Relations for Processing Image Data from Three-dimensional Tactile Sensors Mounted on a Robot Hand," Proc. of the Asian Control Conf., Vol. 3, 1994, pp. 631-634.

[8] Mott, H., Lee, M. H. and Nicholls, H. R., "An Experimental Very-High-Resolution Tactile Sensor Array," in Proc. 4th Int. Conf. On Robot Vision and Sensory Control, 1984, pp. 241-250.

[9] Tanie, K., Komoriya, K., Kaneko M., Tachi, S., and Fujiwara, A., "A High-Resolution Tactile Sensor Array," Robot Sensors Vol. 2: Tactile and Non-Vision, Kempston, UK: IFS (Pubs), 1986, pp. 189-198.

[10] Nicholls, H. R., "Tactile Sensing Using an Optical Transduction Method," Traditional and Non-traditional Robot Sensors (Edited by T. C. Henderson), Springer-Verlag, 1990, pp. 83-99.

[11] Kaneko, M., H. Maekawa, and K. Tanie, Active Tactile Sensing by Robotic Fingers Based on Minimum-External-Sensor-Realization, Proc. of IEEE Int. Conf. on Robotics and Automation, pp. 1289-1294, 1992.

[12] Maekawa, H., Tanie, K., Komoriya, K., Kaneko M., Horiguchi, C., and Sugawara, T., "Development of a Finger-shaped Tactile Sensor and Its Evaluation by Active Touch," Proc. of the 1992 IEEE Int. Conf. on Robotics and Automation, 1992, pp. 1327-1334.

[13] Ohka, M., Mitsuya, Y., Matsunaga, Y., and Takeuchi, S., "Sensing Characteristics of an Optical Three-axis Tactile Sensor Under Combined Loading," Robotica, vol. 22, 2004, pp. 213-221.

[14] Ohka, M., Kawamura, T., Itahashi, T., Miyaoka, T., and Mitsuya, Y., "A Tactile Recognition System Mimicking Human Mechanism for Recognizing Surface Roughness," JSME International Journal, Series C. Vol. 48, No. 2, 2005, pp. 278-285.